




# Global shape of Toll activation is determined by *wntD* enhancer properties

Neta Rahimi<sup>a,1</sup>, Shari Carmon<sup>a,1</sup>, Inna Averbukh<sup>a,1</sup> , Farzaneh Khajouei<sup>b</sup>, Saurabh Sinha<sup>b</sup> , Eyal D. Schejter<sup>a</sup>, Naama Barkai<sup>a</sup>, and Ben-Zion Shilo<sup>a,2</sup> 

<sup>a</sup>Department of Molecular Genetics, Weizmann Institute of Science, Rehovot 761001, Israel; and <sup>b</sup>Department of Computer Science, University of Illinois at Urbana-Champaign, Urbana, IL 61801

Edited by Michael Levine, Princeton University, Princeton, NJ, and approved December 10, 2019 (received for review October 18, 2019)

**Buffering variability in morphogen distribution is essential for reproducible patterning. A theoretically proposed class of mechanisms, termed “distal pinning,” achieves robustness by combining local sensing of morphogen levels with global modulation of gradient spread. Here, we demonstrate a critical role for morphogen sensing by a gene enhancer, which ultimately determines the final global distribution of the morphogen and enables reproducible patterning. Specifically, we show that, while the pattern of Toll activation in the early *Drosophila* embryo is robust to gene dosage of its locally produced regulator, WntD, it is sensitive to a single-nucleotide change in the *wntD* enhancer. Thus, enhancer properties of locally produced WntD directly impinge on the global morphogen profile.**

morphogen gradients | embryogenesis | integral feedback | *Drosophila* | Toll signaling

The profile of morphogen gradients determines the resulting arrays of gene expression that govern embryonic body pattern formation. Buffering variability in morphogen distribution between individual embryos is essential to achieve reproducible patterning. We previously described a general class of mechanisms that buffers variability through “distal pinning,” a global feedback mechanism that continuously modulates the spread of the gradient and concludes only when morphogen value at a distal position reaches some given, fixed level (1–3). Since the feedback acts globally, pinning the morphogen level at one point effectively determines the distribution throughout the field. Thus, the morphogen gradient can withstand fluctuations in the different parameters controlling its establishment. The gradient, however, remains sensitive to the parameters defining its “pinning value,” namely the value at the distal position, the attainment of which terminates the feedback.

We recently suggested that a distal pinning mechanism buffers fluctuations in patterning of the dorso-ventral (DV) axis in early *Drosophila* embryos. Here, the global feedback is exerted by a feedback inhibitor, WntD, the expression of which is restricted to a specific region of the embryo and further depends on the patterning signal itself: the level of nuclear-localized Dorsal protein (4). While *wntD* is expressed locally in the syncytial embryo, it encodes a secreted protein that diffuses readily within the extracellular milieu. WntD is therefore produced as long as nuclear Dorsal is higher than some threshold, defined by the sensitivity of the *wntD* enhancer. Since WntD narrows down the nuclear Dorsal gradient, *wntD* expression eventually stops. Thus, at steady state, the levels of nuclear Dorsal, specifically at the region expressing *wntD*, are “pinned” to the threshold level defined by the *wntD* enhancer. This model therefore predicts, perhaps counterintuitively, that changing the copy number of *wntD* will have no effect on the final gradient, but that modulating *wntD* expression by altering its enhancer will change the global distribution of nuclear Dorsal and therefore perturb patterning. We previously showed that DV axis patterning is indeed robust to changes in *wntD* copy number (4). We next wanted to examine whether changing the endogenous *wntD* enhancer properties would modulate the pattern.

## Results

**Rationale.** Nuclear entry of the transcription factor Dorsal in the early *Drosophila* embryo depends on the Toll pathway. The Toll receptor is activated in a graded manner, instructed by a gradient of its ligand Spätzle (Spz) (5, 6). Expression of the feedback-regulated pathway inhibitor *wntD* is restricted to the termini of the embryo following Torso-induced ERK phosphorylation and removal of the maternally provided ubiquitous transcriptional repressor Capicua (Cic) (Fig. 1A) (7). While *wntD* is expressed locally in the syncytial embryo, it encodes a secreted protein that diffuses readily within the extracellular milieu and acts globally. In addition to binding sites for Cic, the *wntD* enhancer also has binding sites for Dorsal that tune its expression according to the level of Toll activation within each embryo (Fig. 1A–C). WntD binds the Toll receptor and blocks binding of the activating ligand Spz (4). Thus, the levels of WntD tune Toll signaling by regulating the number of available receptors.

WntD is expected to accumulate, and thereby narrow down the Toll activation gradient, until the level of Toll signaling falls below the threshold for *wntD* induction. The *wntD* expression domain that is defined by Torso activation and Cic phosphorylation displays intermediate levels of Toll signaling. It follows that the enhancer landscape of *wntD* is directly related to the final global shape of the Toll activation gradient.

## Significance

**A central issue in robust patterning mediated by morphogens is how to buffer variability in morphogen distribution between embryos. We previously described a class of mechanisms that buffers variability through “distal pinning,” a global feedback mechanism that modulates the spread of the gradient and terminates only when morphogen values at a distal position reach some given, fixed level. We have previously shown in *Drosophila* embryonic dorso-ventral patterning that the secreted WntD protein modulates Toll pathway activation. We have altered the *wntD* enhancer and demonstrate a global contraction of the Toll gradient. The demonstration of a direct link between the enhancer properties of the modulator gene and the morphogen activation profile establishes a molecular mechanism for buffering variability in morphogen distribution.**

Author contributions: N.R., S.C., I.A., E.D.S., N.B., and B.-Z.S. designed research; N.R. and S.C. performed research; S.C., I.A., F.K., and S.S. contributed new reagents/analytic tools; N.R., I.A., F.K., S.S., E.D.S., N.B., and B.-Z.S. analyzed data; and E.D.S., N.B., and B.-Z.S. wrote the paper.

The authors declare no competing interest.

This article is a PNAS Direct Submission.

Published under the PNAS license.

<sup>1</sup>N.R., S.C., and I.A. contributed equally to this work.

<sup>2</sup>To whom correspondence may be addressed. Email: benny.shilo@weizmann.ac.il.

This article contains supporting information online at <https://www.pnas.org/lookup/suppl/doi:10.1073/pnas.1918268117/-DCSupplemental>.

First published January 3, 2020.

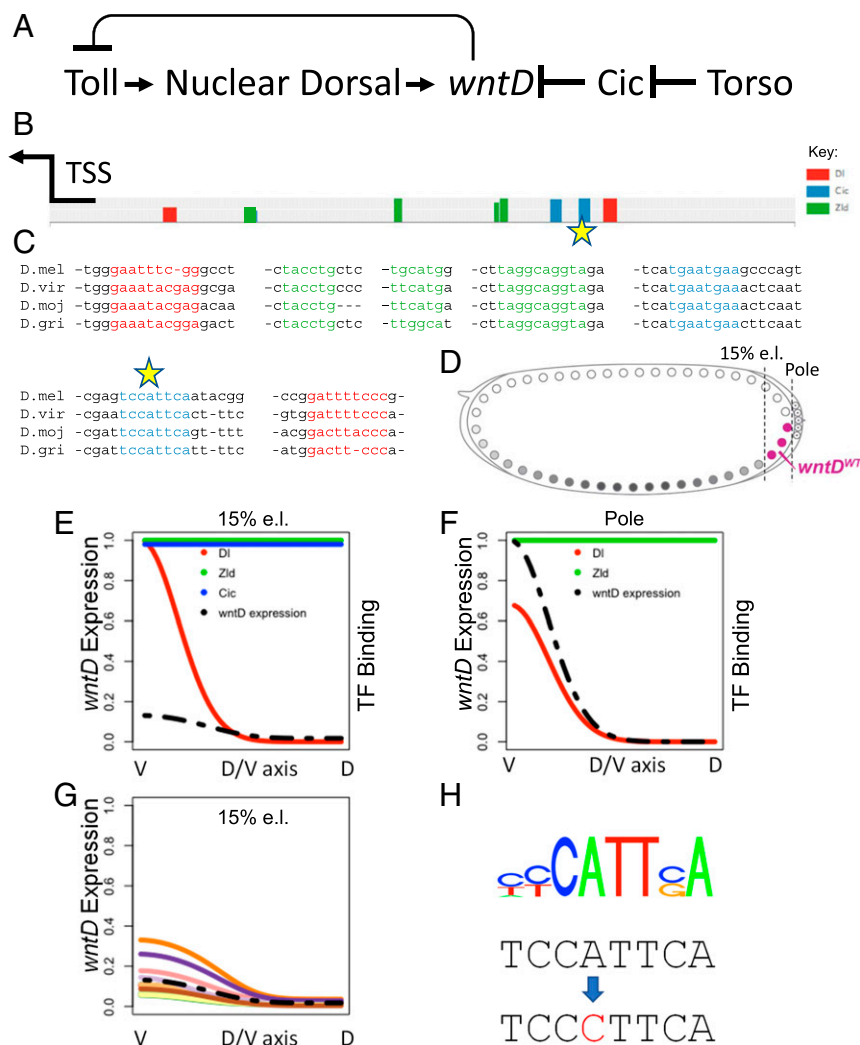


**Fig. 1.** Modeling the *wntD* enhancer. (A) *wntD* expression is triggered by Toll signaling that leads to nuclear targeting of Dorsal and is repressed by Cic binding. Secreted WntD protein in turn attenuates the activation of Toll. (B) Predicted binding sites for the TFs Dorsal (red), Zld (green), and Cic (blue) within the *wntD* enhancer (a 500-bp segment upstream of the *wntD* transcriptional start site), using known motifs for these TFs. The heights of the bars represent predicted site strengths. The arrow marks the transcription-start site (TSS) of *wntD*. (C) Sequence alignment for the binding sites marked in B shows that the sites are highly conserved among evolutionarily distant species (*D. melanogaster*, *D. virilis*, *D. mojavensis*, and *D. grimshawi*). (D) Schematic of the syncytial *D. melanogaster* embryo and *wntD* expression domain (magenta). We modeled the expression profile of *wntD* along the DV axis in 2 different locations, the posterior pole and 15% egg length (e.l.), marked by the vertical dashed lines. The modeling assumes a cylindrical embryo, i.e., the existence of a DV axis at each anterior–posterior position from 0 e.l. to 100% e.l. (E and F) Predicted binding levels of the wild-type *wntD* enhancer by the 3 TFs (colored solid lines), and the resulting *wntD* expression profile (black dashed line) along the DV axis, are shown at 15% e.l. (E) and at the posterior pole (F). Expression levels and TF binding are on a relative scale with maximum expression or binding along the DV axis, across both anterior–posterior positions, being assigned a value of 1. (G) Predicted DV expression profile of *wntD* at 15% e.l. with the selected Cic-binding mutation, using an ensemble of models, predicting an elevated expression. Each line represents the prediction of a cluster of models in the ensemble. The dashed line is the wild-type expression, as shown in E. (H) The selected mutation changes the high-specificity A at position 4 of the distal Cic motif (position –358 of the enhancer) to a C (marked by stars in B and C).

To check this prediction, we sought to alter the sensitivity of the *wntD* enhancer and examine the impact on the final pattern of the Toll activation gradient.

**Compact Organization of the *wntD* Enhancer.** To examine whether changing the activation threshold of *wntD* will modify the global Toll signaling profile, it was necessary to define which sequences in the *wntD* enhancer regulate its activation threshold. We used the thermodynamics-based model generator GEMSTAT (8, 9) to quantitatively describe the combinatorial logic of transcription factor (TF) binding sites within the *wntD* enhancer. The GEMSTAT models identify binding sites for one or more TFs in the enhancer and use the strengths of these sites, as well as cellular concentrations of the TFs, to predict the expression level driven

by that enhancer. Putative binding sites for the TFs Dorsal, Zelda (Zld), and Capicua (Cic), which are highly conserved in diverse *Drosophila* species, were identified within the *wntD* enhancer (Fig. 1C). A subset of the models made predictions consistent with expression data for the wild-type *wntD* enhancer, i.e., little or no detectable expression in the trunk region and a DV patterned expression at the poles (Fig. 1E and F; see also ref. 4).

We then used this subset of models to predict the effect of single-nucleotide mutations in the enhancer, which will alter *wntD* expression levels with minimal disruption to enhancer structure. Specifically, we looked for a way to partially relieve the repression of the *wntD* enhancer by Cic in order to make *wntD* expression more responsive to activation by Dorsal signaling. We

selected such a mutation, located at a key position in the more distal of the 2 Cic-binding sites, which is predicted to strongly diminish the binding to this site. The models vary in their exact assessment of the consequences of this mutation, but the majority agree in predicting de-repression of *wntD* expression in the trunk region due to weakening of the Cic site (Fig. 1 G and H).

**Modulation of One Cic-Binding Site Leads to Broader Expression of *wntD*.** To test if modulation of the distal Cic site within the *wntD* enhancer will indeed expand the normal *wntD* expression domain, we generated 2 transgenic reporter fly lines harboring distinct transcriptional outputs. In one reporter construct, the intact *wntD* enhancer (*wntD*<sup>WT</sup>) drives expression of green fluorescent protein (GFP), while in the second construct, the modified *wntD* enhancer (*wntD*<sup>cic</sup>) drives expression of the murine gene *Atoh1* (10). For accurate comparison, we followed expression of both reporters within the same embryo, collecting embryos at nuclear division cycles 12 through 14. Furthermore, since we wanted to monitor active transcription, rather than accumulation of transcripts over time, we utilized single-molecule RNA fluorescence in situ hybridization (smFISH) for detection. Active transcription is apparent as a strong, focused spot of hybridization within the

nucleus, distinct from the dispersed signal of accumulated transcripts in the cytoplasm (Fig. 2).

Cic protein is maternally provided and uniformly distributed within the embryo (11). Torso signaling at the termini triggers ERK, leading to phosphorylation and nuclear export of Cic. Thus, the *wntD* enhancer is accessible to activation by Dorsal only at the termini. *wntD* transcription at the anterior terminus is delayed since Bicoid competes for phosphorylation by ERK (12). At early time points, when both reporters are expressed, the modified *wntD* enhancer is expected to be less sensitive to repression by Cic and therefore to drive expression in a comparatively larger number of nuclei, occupying a broader domain. Later on, *wntD*<sup>cic</sup> should continue to drive expression at a time when the endogenous enhancer is nearly silent.

We validated both of these predictions in embryos. At nuclear cycle (NC) 13 both reporters are expressed, but the expression of *wntD*<sup>cic</sup>-*Atoh1* encompasses more nuclei (Fig. 2 A and B). By NC 14, expression of *GFP* driven by the *wntD*<sup>WT</sup> enhancer is restricted to a small number of nuclei, while *wntD*<sup>cic</sup> is still driving expression of *Atoh1* in a significant number of nuclei (Fig. 2 D and E). Compilation of data from multiple embryos shows that

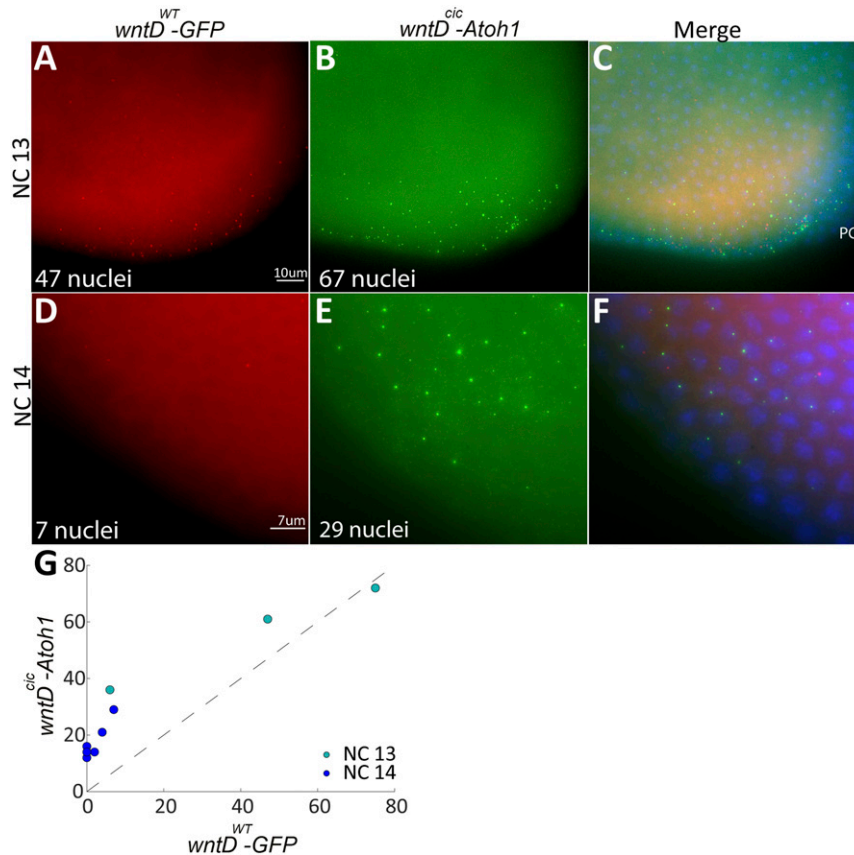


**Fig. 2.** Modulation of a Cic-binding site expands *wntD* expression. Modeling suggested that alteration of a Cic-binding site would expand *wntD* expression. smFISH was used to follow active reporter transcription and compare the expression domains of the wild-type *wntD*<sup>WT</sup> driving *GFP* expression (A and D, red) and a modified *wntD*<sup>cic</sup> enhancer driving mouse *Atoh1* (B and E, green) within staged single embryos. (C and F) The merged images, along with DAPI staining (blue) to visualize the nuclei. PC, pole cells. (A–C) At NC 13, both constructs are expressed at the posterior pole of the embryo, but expression of *Atoh1* via *wntD*<sup>cic</sup> is broader and encompasses more nuclei. (D–F) By NC 14, expression of *GFP* via *wntD*<sup>WT</sup> is almost diminished, indicating that steady state has been reached, while *wntD*<sup>cic</sup> still drives *Atoh1* expression in a significant number of nuclei. (G) Compilation of data from multiple embryos shows that the number of nuclei expressing the *wntD*<sup>cic</sup>-*Atoh1* construct is always higher. Each point on the plot represents an embryo fixed at a specific time point in the embryo. The x axis represents the number of *wntD*-expressing nuclei via the wild-type enhancer while the y axis represents the number of *wntD*-expressing nuclei via the mutant enhancer. The dashed line is the  $x = y$  boundary; therefore, for points above the dashed line, the number of expressing nuclei is greater for the mutant enhancer and vice versa. Two trends are observed: 1) All but one dot are well above the dashed line, indicating a greater amount of expressing nuclei for the mutant enhancer throughout NCs 13 and 14, and 2) The dark blue points depicting NC 14 all show a smaller number of expressing nuclei than the green points displaying NC 13, indicating a decrease in the amount of expressing nuclei between NCs 13 and 14 for both WT and mutant enhancers.

during these nuclear cycles the number of nuclei expressing *Atoh1* via *wntD<sup>cic</sup>* is always larger (Fig. 2G).

**Gastrulation of a Reduced Mesoderm Domain upon Modulation of a Cic-Binding Site.** Since the *wntD<sup>cic</sup>* enhancer reporter is capable of driving a broader and prolonged expression compared to the wild-type enhancer, we wanted to monitor the biological outcomes, following a similar alteration to the expression profile of endogenous *wntD*. We used standard CRISPR methodologies to

modify the endogenous *wntD* enhancer, so that the distal Cic-binding site is compromised similar to the *wntD<sup>cic</sup>* reporter. Embryos harboring this modification are homozygous viable and will be referred to as *wntD<sup>cic</sup>* embryos. Our model predicts that the lower threshold for *wntD<sup>cic</sup>* expression would lead to prolonged expression and give rise to a global reduction in the steady-state distribution of Toll activation gradient. We therefore monitored the distribution of Toll activation in wild-type and *wntD<sup>cic</sup>* embryos using different outputs.

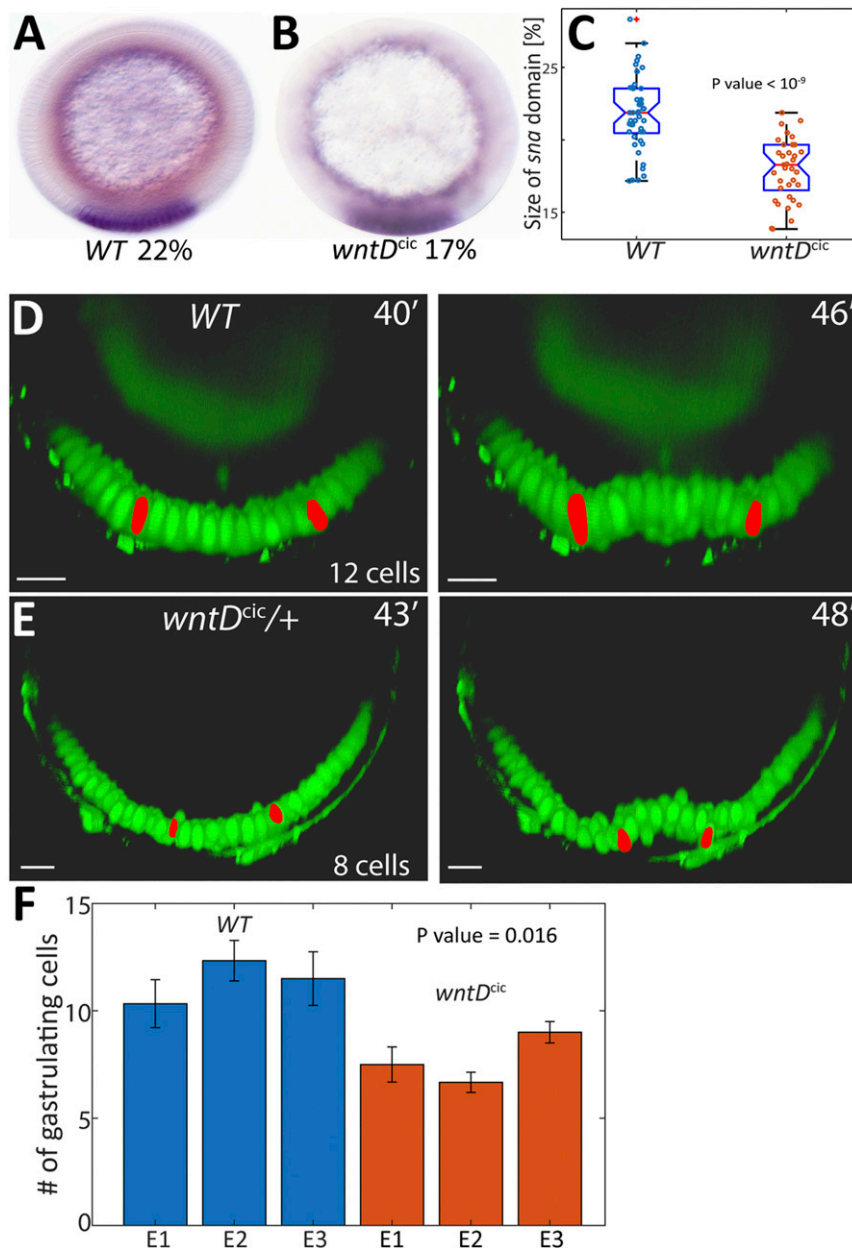


**Fig. 3.** Expanded *wntD* expression alters the global Toll activation profile. (A and B) The circumferential proportion of the domain expressing *sna* (purple ventral stripe) was monitored as a measure for the width of the Toll pathway activation profile. (C) The size of the *sna* domain, measured in multiple embryos, was consistently higher in *wt* embryos than in *wntD<sup>cic</sup>* embryos. Box plots of percent of *sna* domain sizes: Boxed area defines 25 to 75 percentile and the whiskers extend to the most extreme points not considered outliers. Mean is marked by red line. Note that at NC 14, when prominent *sna* expression is induced, expression of *wntD<sup>cic</sup>* did not reach termination and steady state (Fig. 2E). Thus, monitoring *sna* expression is an under-estimate of the capacity of excess WntD levels to influence and restrict Toll pathway activation under these conditions. (D and E) Analysis and comparison of the number of cells undergoing ventral furrowing, monitored by live imaging of Dorsal-GFP (green), which localizes to ventral nuclei, in *wt* and *wntD<sup>cic/+</sup>* embryos. Nuclei at the lateral edges of the ventral furrow (red) served as guideposts for the extent of the gastrulating domain. (F) Quantitation of 3 embryos of each genotype demonstrates that the size of the invagination domain is consistently smaller in *wntD<sup>cic/+</sup>* embryos (*P* value indicated on plots C and F was calculated using unpaired *t* test). Error bars reflect differences in measurement between 3 anterior-posterior locations within each embryo. (Scale bars, 20  $\mu$ m.)

One measure of the activation profile is the expression domain of *snail* (*sna*), a Dorsal-target gene, which typically occupies 22% of the embryo circumference, centered on the ventral midline, in wild-type embryos (13). In homozygous *wntD<sup>cic</sup>* embryos, the *sna* expression domain was reduced to 18% of the circumference (Fig. 3 A–C). Another measure for the Toll-activation pattern is the number of cells undergoing invagination into the ventral furrow at the onset of gastrulation. Expansion of the Toll profile was shown to lead to a broader front of gastrulating cells (14, 15). We thus wanted to examine if the change in *wntD* enhancer properties will give rise to the predicted reduction in the number of gastrulating cells, due to a narrowing of the Toll activation profile. Toward this end, heterozygous *wntD<sup>cic</sup>* embryos carrying a Dorsal-GFP reporter (16) were monitored by live imaging using light sheet fluorescence microscopy. Our earlier work demonstrated that altering the number of wild-type *wntD* copies changes the dynamics but leads to a similar steady-state Toll activation profile (4). We therefore reasoned that a single copy of the modified *wntD<sup>cic</sup>* gene would be sufficient to alter the steady-state profile.

Once gastrulation ensues, the extent of the ventrally furrowing domain—the future mesoderm—can be defined by identifying the most lateral nuclei that alter their orientation. While it is difficult to count the number of gastrulating nuclei once furrow formation initiates, tracing these edge nuclei back in time allows us to score the number of nuclei between them at the earlier monolayer blastoderm stage. Using this approach, we find that the ventrally furrowing domain is indeed significantly and reproducibly smaller in *wntD<sup>cic</sup>/+* heterozygous embryos, dropping from 12 to 8 gastrulating cells (Fig. 3 D–F and *SI Appendix*, Fig. S1).

## Discussion

We examined the consequences of altering the enhancer of the *wntD* gene. We previously suggested that WntD function generates an integral-feedback loop that buffers the global distribution of the Toll-activation gradient (4). Our model assigns a critical role for the enhancer because it determines the fixed point at which transcription of *wntD* will stop and the Toll activation gradient will reach steady state. The model predicts that the gradient is stable to alternation in *wntD* copy number, since each copy is buffered by the very same integral-feedback loop mediated by WntD. In contrast, the gradient is highly sensitive to changes in the *wntD* enhancer that alter the binding sensitivity to its regulators. We previously confirmed that changes in *wntD* gene dosage are indeed of no consequence to the final global pattern (4). Here, we showed that modulation of the endogenous *wntD* enhancer indeed affects the global Toll-activation pattern.

Specifically, we predicted and verified that a single-nucleotide change in the *wntD* enhancer will modify its expression properties, making it less sensitive to repression and thus allowing *wntD* to be expressed in a broader domain and for longer time periods. The consequence is that higher levels of WntD protein are uniformly distributed and accumulate within the perivitelline fluid surrounding the embryo, leading to a global reduction in the steady-state profile of Toll activation. Within the framework of our integral-feedback model, lower levels of nuclear Dorsal are sufficient for activating expression of the modified *wntD* enhancer. Accordingly, its expression will terminate and steady state will be reached, only when the gradient will be further narrowed to reach this new and lower pinned level. Indeed, by monitoring the zygotic output Toll signaling, we showed that the *snail* expression domain, defining the future mesoderm, became narrower. In addition, the number of cells undergoing ventral furrowing was reduced (summarized in Fig. 4).

The enhancer of a gene encoding a secreted modulator plays a critical role with broad implications for achieving robust patterning. Since modulator expression is regulated by the morphogen, it

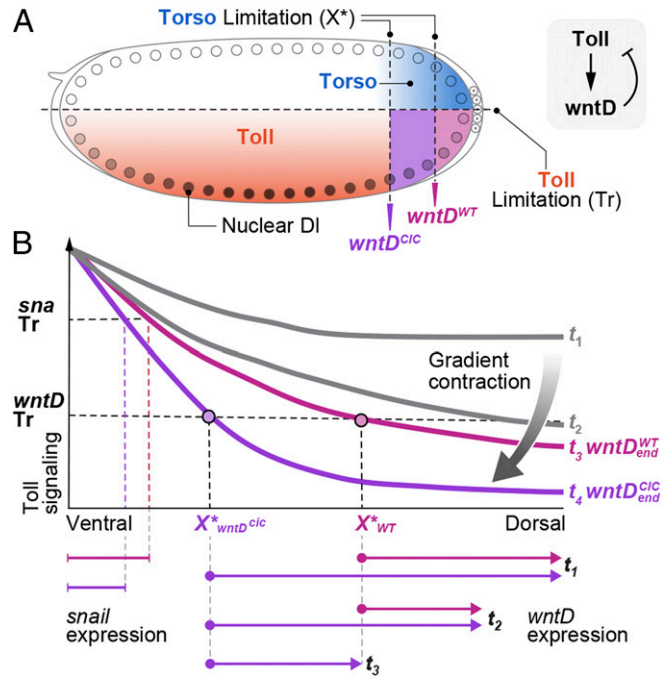


**Fig. 4.** *wntD* enhancer determines the global Toll activation profile. (A) In the syncytial *Drosophila* embryo, the Toll activation gradient is orthogonal to Torso signaling at the termini. Induction of *wntD* expression requires both signals and hence is confined to the termini, where Torso signaling removes the transcriptional repression by Cic. Due to the geometry of the embryo, this domain is exposed to intermediate levels of Toll signaling and displays intermediary levels of Dorsal-nuclear localization, accordingly. Modulation of 1 of the 2 Cic-binding sites in the *wntD* enhancer gave rise to broader and prolonged expression of *wntD*. (B) Early embryos ( $t_1$ ) display an excess of Toll activation manifested by a broad activation profile. This leads to local induction of *wntD* expression only in the restricted *wntD* expression zone which is defined by  $X > X^*$ .  $X^*$  is determined by the *wntD* enhancer and appears in magenta for *wntD<sup>WT</sup>* and purple for *wntD<sup>cic</sup>*. The size of the *wntD* expression domain is determined by Toll-signaling levels, which must be above the threshold ( $Tr$ ) in order to induce *wntD* expression. The *wntD* expression zone is indicated by the arrows below the plot for *wntD<sup>WT</sup>* (magenta) and *wntD<sup>cic</sup>* embryos (purple). The secreted WntD protein is broadly distributed, giving rise to a global contraction of Toll signaling. During the reduction in Toll signaling, the expression of *wntD* is decreased ( $t_2$ ) and is terminated at  $t_3$  (*wntD<sup>WT</sup>*, magenta), when Toll-signaling levels reach steady state and fall below the threshold of *wntD<sup>WT</sup>* induction. *wntD<sup>cic</sup>* embryos (purple) continue to express *wntD* at this point, leading to further contraction of Toll signaling at steady state ( $t_4$ ). The expression domains of target genes such as *sna* are reduced accordingly.

will terminate only when the morphogen profile reaches steady state at a fixed point. This point is determined by the enhancer properties of the modulator and will thus define the final global distribution of the morphogen activation gradient (3). Under this regime, the patterning system can tolerate variability in the initial activation profile, as long as there is sufficient time for production and diffusion of the secreted modulator.

The general concept, whereby enhancers of secreted feedback-regulators play a critical role in shaping patterning gradients, can be executed by diverse molecular mechanisms. In the *Drosophila* wing imaginal disc, distribution of the Dpp morphogen is modulated by the secreted protein Pentagone (Pent) (17). This protein facilitates a longer diffusion range of Dpp by triggering endocytosis of the coreceptors (18). Since *pent* expression is repressed by Dpp signaling, expression will terminate when Dpp signaling levels at the edge of the field reach the fixed point for *pent* repression. This mechanism allows to scale the distribution of the Dpp gradient with the size of the wing disc (2, 19). Recently, the secreted

Scube2 protein was shown to play a similar role during zebrafish neural-tube development in buffering the distribution of the Sonic Hedgehog (Shh) gradient. Due to repression by Shh signaling, Scube2 is expressed only at the edge of the gradient and facilitates the distribution of the morphogen (20). WntD provides another example for the Distal pinning paradigm. In this case, the signals are reversed relative to Pent or Scube2: WntD constricts the activation gradient and is activated by morphogen signaling (4). The restricted *wntD* expression to lower values of the morphogen gradient, which is necessary to avoid complete morphogen signaling shutdown, is achieved by the Torso pathway that confines *wntD* expression to the embryo termini (Fig. 4A).

Secreted proteins that modulate the global morphogen profile represent critical and potent external regulatory knobs that are not part of the core signaling cascade. Fine-tuning their expression properties by enhancer modification may thus impinge on the global morphogen distribution profile without altering the structure of proteins that constitute the primary signaling pathway. During evolution of new species, a single change in the enhancer that drives expression of the secreted modulator may be sufficient to alter the global distribution of a morphogen, and hence the size of the field that will be patterned.

## Methods

**Bioinformatics.** The ensemble of models taken from ref. 9 consists of a set of models, each one being a setting of free parameters of GEMSTAT that accurately predict the DV expression pattern of the wild-type *ind* enhancer using its sequence and the TF concentration profiles of the TFs Dorsal, Zld, and Cic as well as Vnd and Sna. The model relies upon predetermined binding motifs (position weight matrices) of the TFs to identify and quantify binding site strengths in the enhancer. Here, we used an ensemble of models, trained on an enhancer of the gene *intermediate neuroblasts defective (ind)* in our previous work (9), and applied it to the *wntD* enhancer. Binding motifs for Dorsal, Zld, and Cic were obtained from FlyFactorSurvey (21). We used DNaseI hypersensitivity data from stage 5 embryos (22) to identify a 500-bp segment of the *wntD* enhancer that exhibits high levels of DNA accessibility and harbors a cluster of TF-binding sites for Dorsal, Zld, and Cic. We separately predicted *wntD* expression across the DV axis at 15% egg length (same position as that modeled in ref. 9) and at the poles; Zld was assumed to have a uniform concentration profile along the DV axis in both cases, Cic was assumed to be uniformly expressed in the trunk but absent at the poles, and Dorsal was assumed to have a gradient along the DV axis, with the ventral peak expression being higher in the trunk region than at the poles (Fig. 1 E and F). We selected the subset of models, the predictions of which for the wild-type *wntD* enhancer were within a small root-mean-square-deviation (RMSE) of the known expression readout in the trunk and poles. We constructed a probability distribution over these models following the procedure in ref. 9 and computed the predicted effect of each single-nucleotide mutation in the enhancer as the average, over this distribution of the RMSE between predicted DV expression profiles with and without the mutation. An "A" to a "C" mutation at position -358 in the 500-bp enhancer, which targets a high-specificity position in a Cic-binding site and had among the largest predicted effects of any single mutation, was chosen for further study. The *wntD* enhancer sequence used in the analysis is the following: ATGATGAACCGGGTCAGCACATTATAGCTGCAAATCCCA-AGC-CAGGGCCCTCCTGGGGCCGGCCCGTGGGAATTCGGGCCTGCTCAAAA-AACCGGAAATTTCCGCTTTCCACTTGGAATTTTGCATGGGCAGGGGGTAGGA-CTCCCGCAATTGGACGGGTA CAAAAACCCACTGGCAGCCGAGACGCAATTG-CGGAGCAGCCAGTTTCTGGTTGACTACTGCTCTCTGCTGCGCCGGCGGAGG-TGAAGGATCCGCTTCTGCTCGAGCAAGTTTCCACGCTTAGCGAGGTAGAGCCG-TAAACGGCACCCGACGTGCTCATGAATGAAGCCAGTCGAGTCCATTCAATACG-GCCGGATTTCCCGGACTCACTGCAACATCAATGCCGATACGGGGACGGGT-TTGTGGTGGTGGACTGGTCAAGCAATTATATAACAAACATATGACCAACAG-TATATACAGTATAATCTGGGA. The mutation changes the Cic site TCCATCA to TCCCTCA.

**Engineering of Fly Strains.** The *wntD<sup>wt</sup> > GFP*; *wntD<sup>cic</sup> > Atoh1* strain used for single-molecule FISH (smFISH) harbors 2 reporter transgenes. The *wntD<sup>wt</sup> > GFP* reporter was generated by synthesizing a DNA construct which included the 1,162-bp region upstream of the *wntD* transcription start site followed by the coding region of superfolder GFP (23). *wntD<sup>cic</sup> > Atoh1* was generated by replacing the wild-type enhancer and GFP sequences

with a synthesized sequence which included the *wntD<sup>cic</sup>* enhancer and the coding sequence of murine *Atoh1* (10). Both constructs were inserted into UASp-attB plasmids and integrated into the chromosomal AttP40 and AttP2 sites, respectively.

The *wntD<sup>cic</sup>* strain was generated by CRISPR-induced replacement of the entire *wntD* gene with a sequence that contains an A > C point mutation at position 4 of the distal *cic*-binding site (Fig. 1H). We used the following oligonucleotide pairs to generate the relevant guide RNAs: CTTCGAAAC-CACCTGTAGCTAAAAC, AAACGTTTTAGCTACAGGTGGTTTC; and CTTCGAAGTCC-TGTCTGCGTAGCAC; AAACGTGCTACGACAGGACTTC.

To follow the ventrally invaginating cells during gastrulation, we used *Sco*/CyO; *dorsal*-GFP/TM3, *Sb* flies (16), a strain in which the ventral nuclei are labeled by a Dorsal-GFP fusion protein.

**smFISH.** A Stellaris RNA FISH probe set for the sfGFP gene was designed by Stellaris Probe Designer and labeled with Quasar670 from LGC Biosearch Technologies. The probe set for the murine *Atoh1* gene, labeled with Texas Red, was a gift from the S. Itzkovitz laboratory, Weizmann Institute, Rehovot, Israel. smFISH was carried out as in Rahimi et al. (15). Embryos carrying both reporter constructs were collected for 1 h after egg laying followed by a 2-h incubation, fixed for 25 min in 4% formaldehyde, washed in methanol, and kept at -20 °C. Next-day embryos were washed in methanol and then in ethanol, rocked in 90% Xylene, 10% ethanol for 1 h followed by post-fixation and then incubated 6 min with Proteinase K and postfixed again. Embryos were transferred gradually to 10% formamide (deionized) (FA) in 2× Saline Sodium-Citrate buffer (SSC) + 10 µg/mL single-stranded DNA (ssDNA) preheated to 37 °C and prehybridized for 30 min at 37 °C. Hybridization buffer included 10% FA, 10% Dextran, 2 mg/mL bovine serum albumin, ribonucleoside vanadyl complex (RVC), and ssDNA + transfer RNA in 2× SSC, containing the probe set (1 ng/µL) (24). Hybridization was carried out overnight at 37 °C. Next day the embryos were shaken gently and incubated for another 30 min. Embryos were washed twice for 30 min at 37 °C with 10% FA in 2× SSC + 10 µg/mL ssDNA and gradually transferred to phosphate-buffered saline/0.5% Tween and mounted with Vectashield + DAPI Mounting Medium (Vector Laboratories Inc.). Fluorescence was visualized with a Nikon Eclipse Ti2 microscope and analyzed by the TransQuant script as was previously described (25).

**Snail In Situ Hybridization and Expression Domain Quantitation.** In situ hybridization for *sna* was carried out as in Rahimi et al. (4). Fixation of the embryos was carried out in 4% paraformaldehyde, and probe hybridization was carried out at 55 °C. The expression domain was detected via a digoxigenin (DIG)-labeled DNA probe, followed by anti-DIG-alkaline phosphatase-conjugated antibody and substrate detection (Roche), and visualized following cross-sectioning in the middle of the embryo using a tungsten needle. Quantitation of the relative size of the *sna* domain of the full-embryo circumference was carried out using a MATLAB script that manually identifies the expression domain and calculates the angle generated from the center divided by 360.

**Light Sheet Fluorescence Microscopy and Quantitation of Ventral Furrowing.** Embryos were imaged using a Light Sheet Z.1 microscope (Zeiss Ltd.) equipped with 2 sCMOS cameras PCO-Edge, 10× excitation objectives, and Light Sheet Z.1 detection optics 20×/1.0 (water immersion). The embryos were collected and dechorionated, and up to 4 embryos were sequentially mounted perpendicularly into a glass capillary in a 1% low-melting agarose solution. Imaging was performed using dual-side illumination, zoom ×0.8 (GFP excitation: 488 nm; emission/detection: bandpass (BP) 505 to 545; Texas Red excitation: 561 nm, emission/detection: BP 575 to 615 nm).

Optical cross-sections were generated using the Imaris program. The edges of the furrow were defined by marking the 2 lateral-most nuclei that alter their angle with respect to the embryo circumference upon gastrulation. The time-lapse movie was then played backward to an earlier phase of NC 14, when the nuclei are still in a monolayer, in order to accurately count the number of furrowed nuclei.

All data are contained in the manuscript text and *SI Appendix*.

**ACKNOWLEDGMENTS.** We thank S. Ben-Moshe, K. Bahar Halpern, and S. Itzkovitz for advice on smFISH and Y. Addadi and O. Golani for help in acquisition and analysis of light sheet fluorescence microscopy images. Imaging using the light sheet fluorescence microscope was made possible thanks to the de Picciotto-Lesser Cell Observatory founded in memory of Wolf and Ruth Lesser. We thank members of the B.-Z.S. and N.B. laboratories for fruitful discussions. This work was supported in part by NIH Grants R01 GM114341 and R35 GM131819 (to S.S.); United States-Israel Binational

Science Foundation Grant 2017055 (to N.B.); United States-Israel Binational Science Foundation Grant 2015063 (to E.D.S. and B.-Z.S.); and a research grant from the Henry Chanoch Kreuter Institute for Biomedical Imaging

and Genomics (to B.-Z.S.). N.B. is the incumbent of the Lorna Greenberg Scherzer Professorial Chair, and B.-Z.S. is the incumbent of the Hilda and Cecil Lewis Professorial Chair in Molecular Genetics.

1. D. Ben-Zvi, N. Barkai, Scaling of morphogen gradients by an expansion-repression integral feedback control. *Proc. Natl. Acad. Sci. U.S.A.* **107**, 6924–6929 (2010).
2. D. Ben-Zvi, G. Pyrowolakis, N. Barkai, B. Z. Shilo, Expansion-repression mechanism for scaling the Dpp activation gradient in *Drosophila* wing imaginal discs. *Curr. Biol.* **21**, 1391–1396 (2011).
3. B. Z. Shilo, N. Barkai, Buffering global variability of morphogen gradients. *Dev. Cell* **40**, 429–438 (2017).
4. N. Rahimi *et al.*, A WntD-dependent integral feedback loop attenuates variability in *Drosophila* Toll signaling. *Dev. Cell* **36**, 401–414 (2016).
5. M. Haskel-Ittah *et al.*, Self-organized shuttling: Generating sharp dorsoventral polarity in the early *Drosophila* embryo. *Cell* **150**, 1016–1028 (2012).
6. D. Stein, S. Roth, E. Vogelsang, C. Nüsslein-Volhard, The polarity of the dorsoventral axis in the *Drosophila* embryo is defined by an extracellular signal. *Cell* **65**, 725–735 (1991).
7. A. Helman *et al.*, RTK signaling modulates the Dorsal gradient. *Development* **139**, 3032–3039 (2012).
8. X. He, M. A. Samee, C. Blatti, S. Sinha, Thermodynamics-based models of transcriptional regulation by enhancers: The roles of synergistic activation, cooperative binding and short-range repression. *PLoS Comput. Biol.* **6**, e1000935 (2010).
9. F. Khajouei, S. Sinha, An information theoretic treatment of sequence-to-expression modeling. *PLoS Comput. Biol.* **14**, e1006459 (2018).
10. G. Tomic *et al.*, Phospho-regulation of ATOH1 is required for plasticity of secretory progenitors and tissue regeneration. *Cell Stem Cell* **23**, 436–443.e7 (2018).
11. B. Lim *et al.*, Kinetics of gene derepression by ERK signaling. *Proc. Natl. Acad. Sci. U.S.A.* **110**, 10330–10335 (2013).
12. Y. Kim *et al.*, Gene regulation by MAPK substrate competition. *Dev. Cell* **20**, 880–887 (2011).
13. J. Rusch, M. Levine, Threshold responses to the dorsal regulatory gradient and the subdivision of primary tissue territories in the *Drosophila* embryo. *Curr. Opin. Genet. Dev.* **6**, 416–423 (1996).
14. N. C. Heer *et al.*, Actomyosin-based tissue folding requires a multicellular myosin gradient. *Development* **144**, 1876–1886 (2017).
15. N. Rahimi *et al.*, Dynamics of Spatzle morphogen shuttling in the *Drosophila* embryo shapes gastrulation patterning. *Development* **146**, dev181487 (2019).
16. R. DeLotto, Y. DeLotto, R. Steward, J. Lippincott-Schwartz, Nucleocytoplasmic shuttling mediates the dynamic maintenance of nuclear Dorsal levels during *Drosophila* embryogenesis. *Development* **134**, 4233–4241 (2007).
17. R. Vuilleumier *et al.*, Control of Dpp morphogen signalling by a secreted feedback regulator. *Nat. Cell Biol.* **12**, 611–617 (2010).
18. M. Norman, R. Vuilleumier, A. Springhorn, J. Gawlik, G. Pyrowolakis, Pentagone internalises glypicans to fine-tune multiple signalling pathways. *eLife* **5**, e13301 (2016).
19. F. Hamaratoglu, A. M. de Lachapelle, G. Pyrowolakis, S. Bergmann, M. Affolter, Dpp signaling activity requires Pentagone to scale with tissue size in the growing *Drosophila* wing imaginal disc. *PLoS Biol.* **9**, e1001182 (2011).
20. Z. M. Collins, K. Ishimatsu, T. Y. C. Tsai, M. G. Megason, A Scube2-Shh feedback loop links morphogen release to morphogen signaling to enable scale invariant patterning of the ventral neural tube. *bioRxiv*: 10.1101/469239 (13 November 2018).
21. L. J. Zhu *et al.*, FlyFactorSurvey: A database of *Drosophila* transcription factor binding specificities determined using the bacterial one-hybrid system. *Nucleic Acids Res.* **39**, D111–D117 (2011).
22. X. Y. Li *et al.*, The role of chromatin accessibility in directing the widespread, overlapping patterns of *Drosophila* transcription factor binding. *Genome Biol.* **12**, R34 (2011).
23. J. D. Pédelacq, S. Cabantous, T. Tran, T. C. Terwilliger, G. S. Waldo, Engineering and characterization of a superfolder green fluorescent protein. *Nat. Biotechnol.* **24**, 79–88 (2006).
24. T. Trcek, T. Lionnet, H. Shroff, R. Lehmann, mRNA quantification using single-molecule FISH in *Drosophila* embryos. *Nat. Protoc.* **12**, 1326–1348 (2017).
25. K. Bahar Halpern, S. Itzkovitz, Single molecule approaches for quantifying transcription and degradation rates in intact mammalian tissues. *Methods* **98**, 134–142 (2016).